Langmuir Monolayer Properties of Perfluorinated Double Long-Chain Salts with Divalent Counterions of Separate Electric Charge at the Air−Water Interface

Yuki Matsumoto,[†] Hiromichi Nakahara,[†] Yoshikiyo Moroi,[†] and Osamu Shibata*[,†,‡]

Division of Biointerfacial Science, Graduate School of Pharmaceutical Sciences, Kyushu University; 3-1-1 Maidashi, Higashi-ku, Fukuoka 812-8582, Japan, and Department of Biophysical Chemistry, Faculty of Pharmaceutical Sciences, Nagasaki International University, 2825-7 Huis Ten Bosch, Sasebo, Nagasaki 859-3298, Japan

Received February 21, 2007. In Final Form: June 22, 2007

The novel perfluorinated double long-chain salts with divalent counterions of separate electric charge, 1,1-(1,ω-alkanediyl)-bispyridinium perfluorotetradecane- carboxylate [C*n*BP(FC14)$_2$: $n = 2, 6, 10, 14$], were newly synthesized and their interfacial behavior was investigated by Langmuir monolayer methods. Surface properties [surface pressure (π)−, surface potential (ΔV)−, dipole moment ($\mu_\perp$)−area (A) isotherms] and morphological images of C*n*BP(FC14)$_2$ monolayers on a subphase of water and on various NaCl concentrations were measured by employing the Wilhelmy method, the ionizing electrode method, fluorescence microscopy (FM), and Brewster angle microscopy (BAM). C*n*BP(FC14)$_2$ formed a stable monolayer on water at 298.2 K, where these $\pi-A$ isotherms shifted to a larger molecular area with increasing charge separation and had no transition point from a disordered phase to an ordered one. On the contrary, the $\pi-A$ isotherms on NaCl solutions moved to the smaller areas, showed the transition and higher collapse pressures compared to the $\pi-A$ isotherms on water. These results suggested that a sodium chloride subphase induced the condensation of C*n*BP(FC14)$_2$ molecules upon compression. In addition, it is quite noticeable that a dissociation of C*n*BP counterion from C*n*BP(FC14)$_2$ occurs on NaCl solutions, depending on the extent of charge separation. This phenomenon was supported by the changes of the limiting area, transition pressure, collapse pressure, repeated compression−expansion cycle curve, and ΔV behavior of perfluorotetradecanoic acid (FC14). Furthermore, temperature dependence of these monolayers was investigated, and an apparent molar quantity change on the phase transition was evaluated on 0.15 M NaCl. The morphological behavior of C*n*BP(FC14)$_2$ and FC14 monolayers was also confirmed by FM and BAM images.

Introduction

A fluorocarbon has unique features such as hydrophobicity and lipophobicity simultaneously. Fluorinated amphiphiles show different and superior behavior in the bulk and at the air−water interface compared with conventional hydrogenated ones.[1] In general, fluorinated surfactants can be classified into the following two types: perfluorinated surfactants and partially fluorinated surfactants including gemini compounds. A substitution of fluorine for hydrogen changes the surfactant properties drastically.[1] Both the extent of fluorination and the position of fluorine atoms in a molecule affect characteristics of surfactants such as solution properties and interfacial behavior.[2−5] Fluorinated surfactants have higher surface activity and can lower the surface tension of water down to less than 20 mN m^{-1}. For example, only 10 ppm fluorinated surfactant solution can accompany the reduction in the surface tension.[1] In addition, their C−F bond is very stable to acids, alkali, oxidation, reduction, and temperature. Therefore, great attention is being paid to fluorinated surfactants in various fields such as industry[6−8] and the biomedical field.[9−11]

Gemini amphiphiles,[12] which consist of two hydrophobic chains connected in a covalent bond by a spacer, such as bola amphiphiles,[13,14] demonstrate outstanding behavior in two-dimensional (2-D) and three-dimensional (3-D) states.[15−18] They have higher micelle-forming ability and higher surface activity than ordinary hydrogenated amphiphiles. Thus, they are ecofriendly substances, meaning that even small amounts generate the effective ability. Recently, some gemini amphiphiles have been found to possess high transfection activities by containing DNA molecules in their vesicles.[19−21] Moreover, it was reported

* Corresponding author. Department of Biophysical Chemistry, Faculty of Pharmaceutical Sciences, Nagasaki International University; 2825-7 Huis Ten Bosch, Sasebo, Nagasaki 859-3298, Japan. E-mail: wosamu@niu.ac.jp, URL: http://www.niu.ac.jp/∼pharm1/lab/physchem/index.html.

† Kyushu University.

‡ Nagasaki International University.

(1) Kissa, E. *Fluorinated Surfactants and Repellents*, 2nd ed. revised and expanded; Surfactant Science Series, Vol. 97; Marcel Dekker Inc.: Basel, New York, 2001; pp 1−615.
(2) Lehmler, H.-J.; Jay, M.; Bummer, P. M. *Langmuir* **2000**, *16*, 10161−10166.
(3) Broniatowski, M.; Dynarowicz-Latka, P. *Langmuir* **2006**, *22*, 6622−6628.
(4) Broniatowski, M.; Dynarowicz-Latka, P. *Langmuir* **2006**, *22*, 2691−2696.
(5) Broniatowski, M.; Romeu, N. V.; Dynarowicz-Latka, P. *J. Phys. Chem. B* **2006**, *110*, 3078−3087.
(6) Ueno, M.; Ugajin, Y.; Horie, K.; Nishimura, T. *J. Appl. Polym. Sci.* **1990**, *39*, 967−977.
(7) Koller, A.; Bleckmann, A.; Kroepke, R. DE. Patent 99, 19943436, 19943436, 2001.
(8) Nishihama, S.; Sawada, H. J. P. Patent 2003, 285820, 2005053736, 2005.
(9) Riess, J. G.; Le Blanc, M. *Angew. Chem.* **1978**, *90*, 654−668.
(10) Riess, J. G. *Colloids Surf., A* **1994**, *84*, 33−48.
(11) Riess, J. G.; Krafft, M. P. *Biomaterials* **1998**, *19*, 1529−1539.
(12) Menger, F. M.; Keiper, J. S. *Angew. Chem.* **2000**, *39*, 1907−1920.
(13) Escamilla, G. H.; Newkome, G. R. *Angew. Chem.* **1994**, *106*, 2013−2016.
(14) Fuhrhop, J.-H.; Wang, T. *Chem. Rev.* **2004**, *104*, 2901−2937.
(15) Fuhrhop, J. H.; Fritsch, D. *Acc. Chem. Res.* **1986**, *19*, 130−137.
(16) Menger, F. M.; Littau, C. A. *J. Am. Chem. Soc.* **1991**, *113*, 1451−1452.
(17) Menger, F. M.; Mbadugha, B. N. A. *J. Am. Chem. Soc.* **2001**, *123*, 875−885.
(18) Zana, R. *Adv. Colloid Interface Sci.* **2002**, *97*, 205−253.
(19) Camilleri, P.; Kremer, A.; Edwards, A. J.; Jennings, K. H.; Jenkins, O.; Marshall, I.; Neville, W.; Rice, S. Q.; Smith, R. J.; Wilkinson, M. J.; McGregor, C.; Kirby, A. J. *Chem. Commun.* **2000**, 1253−1254.
(20) McGregor, C.; Perrin, C.; Monck, M.; Camilleri, P.; Kirby, A. J. *J. Am. Chem. Soc.* **2001**, *123*, 6215−6220.

10.1021/la700511r CCC: $37.00
Published on Web 08/15/2007

that gemini amphiphiles forming rod-like micelles can be used as templates for preparation of nanoparticles.[22,23] Changes in spacer length or species in a molecule improve and control these unique features. Therefore, in the field of material science much attention is also paid to these amphiphiles with spacers; that is, some papers on fluorinated gemini surfactants have been reported.[24−29] As far as we know, a few papers concerning Langmuir monolayers of gemini amphiphiles have been reported.[30,31]

The surface properties of hydrogenated double long-chain salts with a hydrocarbon spacer have been investigated previously.[32] Notice that the monolayers indicated different transition modes on compression from those of normal aliphatic compounds. Hence, in the present study, perfluorinated double long-chain salts with divalent counterions of separate electric charge or various hydrocarbon spacer lengths (C*n*BP(FC14)$_2$, $n = 2, 6, 10, 14$) were newly synthesized, and then the monolayer properties were investigated to understand the effect on their interfacial behavior of extending charge separation or the spacer length. Surface pressure (π)−, surface potential (ΔV)−, and dipole moment ($\mu_\perp$)−area (A) isotherms of C*n*BP(FC14)$_2$ were obtained on water and on NaCl aqueous solutions of the different concentrations. Thermodynamic quantities of transition from disordered to ordered phase were evaluated from the temperature dependence of the transition pressure.[32−36] Then the results were compared with those of hydrocarbon analogues.[32] Furthermore, the monolayers were also morphologically investigated using Brewster angle microscopy (BAM) and fluorescence microscopy (FM).

Experimental Section

Materials. Perfluorotetradecanoic acid (FC14) was purchased from Fluorochem (United Kingdom) and purified by thrice recrystallization from *n*-hexane/acetone mixed solvent. Fluorescence probe of 1-palmitoyl-2-[6-[(7-nitro-2−1,3-benzoxadiazol-4-yl)amino] hexanoyl]-*sn*-glycero-3-phosphocholine (NBD-PC) was bought from Avanti Polar Lipids, Inc. (Birmingham, AL). 1,1′-(1,ω-Alkanediyl)-bispyridinium bromide and chloride (abbreviation: C*n*BP; $n = 2$, 6, 10, 14) were the kind gifts from the former Kuwamura's laboratory of Gunnma University.[32,37,38] The chemical structures of 1,1-(1,ω-alkanediyl)-bispyridinium perfluorotetradecanecarboxylate (abbreviation: C*n*BP(FC14)$_2$; $n = 2$, 6, 10, 14) used in the present study

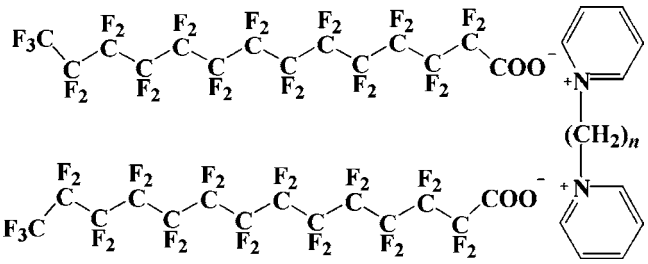

Figure 1. Chemical structures of C*n*BP(FC14)$_2$; $n = 2$, 6, 10, 14.

Table 1. Elemental Analysis of C*n*BP(FC14)$_2$; $n = 2,6,10,14$

surfactant		C (%)	H (%)	N (%)
C14BP(FC2)$_2$	calcd	29.79	0.88	1.74
	found	29.66	0.70	1.92
C14BP(FC6)$_2$	calcd	31.67	1.33	1.68
	found	31.42	1.20	1.62
C14BP(FC10)$_2$	calcd	33.43	1.75	1.62
	found	33.77	1.60	1.76
C14BP(FC14)$_2$	calcd	35.07	2.15	1.57
	found	34.99	2.10	1.78

are shown in Figure 1. These materials were synthesized according to the following procedure. First, FC14 was converted into the corresponding lithium salt by the addition of equimolar lithium hydroxide in aqueous solution. Second, the resultant FC14 lithium salt was mixed with C*n*BP ion, and then the crude materials of C*n*BP(FC14)$_2$ were precipitated. Finally, they were purified by more than thrice recrystallization from the *n*-hexane/ethanol/methanol mixed solvents, and their purities were checked by elemental analysis (see Table 1). *n*-Hexane (Merck (Uvasol), 99.5%), methanol (Merck (Uvasol), 99.7%), ethanol (nacalai tesque, 99.5%), 2,2,2-trifluoroethanol (Wako Chemical, >99.0%), and dichloromethane (Wako Pure Chemical Industries, >99.0%) were used as spreading solvents. Sodium chloride (nacalai tesque) was roasted at 1023 K for 24 h to remove any surface active organic impurity. The substrate solutions of sodium chloride were prepared using thrice distilled water (surface tension = 71.96 mN m^{-1} at 298.2 K, and electrical resistivity = 18 MΩ cm).

Methods

Surface Pressure−Area Isotherms. The surface pressure (π) of monolayers was measured using an automated homemade Wilhelmy film balance, which is the same as that used in the previous studies.[39,40] The surface pressure balance (Mettler Toledo, AG-245) has a resolution of 0.01 mN m^{-1}. The surface measuring system was equipped with the filter paper (Whatman 541, periphery = 4 cm). The trough was made from a 48 cm × 15 cm = 720 cm^2 Teflon-coated brass. The temperature of the substrate was controlled within ± 0.1 K at the desired temperature by circulating thermostated water. Stock solutions of C*n*BP(FC14)$_2$ (0.5 mM) were prepared in dichloromethane/*n*-hexane/2,2,2-trifluoroethanol (5:3:1 v/v for $n = 2$) and *n*-hexane/ethanol/methanol (4:1:1 v/v for $n = 6, 10, 14$). The spreading solvents were allowed to evaporate for 15 min prior to compression. The monolayer was compressed at a speed of ∼0.10 and <0.30 nm^2 molecule^{-1} min^{-1} for FC14 and C*n*BP(FC14)$_2$, respectively.

Surface Potential Measurements. The surface potential (ΔV) was also recorded while the monolayer was compressed. It was monitored using an ^{241}Am electrode at 1−2 mm above the interface while a reference electrode dipped in the subphase. The standard deviations for area and surface potential measurements were ∼0.01 nm^2 and ∼5 mV, respectively.

(21) Kirby, A. J.; Camilleri, P.; Engberts, J. B. F. N.; Feiters, M. C.; Nolte, R. J. M.; Soderman, O.; Bergsma, M.; Bell, P. C.; Fielden, M. L.; Garcia Rodriguez, C. L.; Guedat, P.; Kremer, A.; McGregor, C.; Perrin, C.; Ronsin, G.; van Eijk, M. C. P. *Angew. Chem.* **2003**, *42*, 1448−1457.
(22) Esumi, K.; Hara, J.; Aihara, N.; Usui, K.; Torigoe, K. *J. Colloid Interface Sci.* **1998**, *208*, 578−581.
(23) Bonilla, G.; Diaz, I.; Tsapatsis, M.; Jeong, H.-K.; Lee, Y.; Vlachos, D. G. *Chem. Mater.* **2004**, *16*, 5697−5705.
(24) Menger, F. M.; Littau, C. A. *J. Am. Chem. Soc.* **1993**, *115*, 10083−10090.
(25) Zana, R. *Curr. Opin. Colloid Interface Sci.* **1996**, *1*, 566−571.
(26) Li, Y.; Li, P.; Wang, J.; Wang, Y.; Yan, H.; Dong, C.; Thomas, R. K. *J. Colloid Interface Sci.* **2005**, *287*, 333−337.
(27) Asakawa, T.; Okada, T.; Hayasaka, T.; Kuwamoto, K.; Ohta, A.; Miyagishi, S. *Langmuir* **2006**, *22*, 6053−6055.
(28) Song, X.; Li, P.; Wang, Y.; Dong, C.; Thomas, R. K. *J. Colloid Interface Sci.* **2006**, *304*, 37−44.
(29) Yoshimura, T.; Ohno, A.; Esumi, K. *Langmuir* **2006**, *22*, 4643−4648.
(30) Nishida, J.; Brizard, A.; Desbat, B.; Oda, R. *J. Colloid Interface Sci.* **2005**, *284*, 298−305.
(31) Zhai, X.; Liu, M. *J. Colloid Interface Sci.* **2006**, *295*, 181−187.
(32) Shibata, O.; Moroi, Y.; Saito, M.; Matuura, R. *J. Colloid Interface Sci.* **1991**, *142*, 535−543.
(33) Shibata, O. *J. Colloid Interface Sci.* **1983**, *96*, 182−191.
(34) Shibata, O.; Kaneshina, S.; Nakamura, M.; Matuura, R. *J. Colloid Interface Sci.* **1983**, *95*, 87−96.
(35) Shibata, O.; Kaneshina, S.; Matuura, R. *Bull. Chem. Soc. Jpn.* **1988**, *61*, 3077−3082.
(36) Rusdi, M.; Moroi, Y.; Nakamura, S.; Shibata, O.; Abe, Y.; Takahashi, T. *J. Colloid Interface Sci.* **2001**, *243*, 370−381.
(37) Moroi, Y.; Matuura, R.; Kuwamura, T.; Inokuma, S. *J. Colloid Interface Sci.* **1986**, *113*, 225−231.
(38) Moroi, Y.; Matuura, R.; Tanaka, M.; Murata, Y.; Aikawa, Y.; Furutani, E.; Kuwamura, T.; Takahashi, H.; Inokuma, S. *J. Phys. Chem.* **1990**, *94*, 842−845.
(39) Hoda, K.; Nakahara, H.; Nakamura, S.; Nagadome, S.; Sugihara, G.; Yoshino, N.; Shibata, O. *Colloids Surf. B* **2006**, *47*, 165−175.
(40) Nakahara, H.; Nakamura, S.; Hiranita, T.; Kawasaki, H.; Lee, S.; Sugihara, G.; Shibata, O. *Langmuir* **2006**, *22*, 1182−1192.

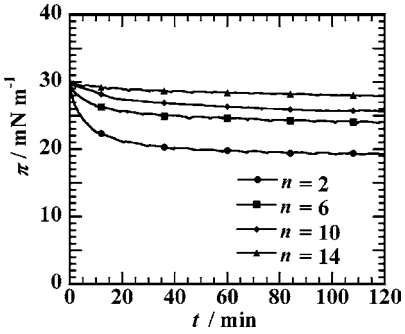

Figure 2. Time dependence of surface pressure (π) for C*n*BP-(FC14)$_2$ monolayers (n = 2, 6, 10, 14) on water at 298.2 K at the fixed molecular areas, where the Langmuir monolayers were compressed up to 30 mN m^{-1} and then the $\pi-t$ measurements were started.

Brewster Angle Microscopy (BAM). The monolayer was directly visualized by a Brewster angle microscope (KSV Optrel BAM 300, KSV Instruments Ltd., Finland) coupled to a commercially available film balance system (KSV Minitrough, KSV Instruments Ltd., Finland). The application of a 20-mW He−Ne laser of emitting *p*-polarized light of 632.8 nm wavelength and 10× objective allowed a lateral resolution of ~2 μm. The angle of the incident beam to the air−water interface was fixed to Brewster angle (53.1°) at 298.2 K. The reflected beam was recorded with a high-grade CCD camera (EHDkamPro02, EHD imaging GmbH, Germany), and then the BAM images were digitally saved to the computer hard disk.

Fluorescence Microscopy (FM). The film balance system (KSV Minitrough) was mounted onto the stage of the Olympus microscope BX51WI (Tokyo, Japan) equipped with a 100-W mercury lamp (USH-1030L), an objective lens (SLMPlan50×, working distance = 15 mm), and a 3CCD camera with a camera control unit (IK-TU51CU, Toshiba, Japan). The *z*-directional focus on the monolayer was exactly adjusted using an automation controller (MAC 5000, Ludl Electronic Products Ltd., NY). FM observations and compression isotherm measurements were carried out simultaneously. A spreading solution of C*n*BP(FC14)$_2$ was prepared as a mixed solution doped with 1 mol % of a fluorescence probe (NBD-PC). The excitation (460 nm) and emission (534 nm) wavelength were selected by a mirror unit (U-MWIBA3). FM micrographs were directly recorded with the hard disk via an online image processor (DVgate Plus, Sony Corp., Japan) connected to the microscope. Image processing and analysis were carried out by using the software, Scion Image Beta 4.02 for Windows (Scion Corp., Frederick, MD). The total amount of ordered domains was evaluated and expressed as a percentage per frame by dividing the respective frame into dark and bright regions.

Results and Discussion

Stability of C*n*BP(FC14)$_2$ Monolayers. To find out whether C*n*BP(FC14)$_2$ can form stable Langmuir monolayers at the air−water interface, their $\pi-t$ isotherms were investigated on water subphases at 298.2 K. Their monolayers were compressed up to 30 mN m^{-1}, and then the Teflon barrier was stopped, after which relaxation of surface pressure was traced against time (Figure 2). The surface pressures decreased from 30 mN m^{-1} during the first 40 min. Subsequently, they reached almost constant values. That is, the values for C*n*BP(FC14)$_2$ (n = 2, 6, 10, 14) are 19, 24, 25.5, and 28 mN m^{-1}, respectively. The difference between these values can be attributed to the monolayer properties such as disordered- and ordered-type films, which could be determined by Langmuir isotherms and morphological observations as mentioned later. Judging from these results, the $\pi-t$ isotherms demonstrate that all of the materials used here can form stable monolayers at the air−water interface.

Surface Pressure−, Surface Potential−, and Dipole Moment−Area Isotherms. The $\pi-$, $\Delta V-$, and $\mu_\perp-A$ isotherms of C*n*BP(FC14)$_2$ monolayers spread on water at 298.2 K are shown in Figure 3. The materials used in this study have the hydrophobic part of two perfluorocarbon chains and the hydrophilic part with separate electric charges and with one hydrocarbon spacer, whose chain length is variable. Their chemical bond is based on electrostatic interaction. Surface potential for all of C*n*BP(FC14)$_2$ compounds indicated negative values on compression, which is similar to the behavior of analogous substances reported in the previous study,[32] suggesting that the two fluorinated chains act as a hydrophobic part of monolayers. The $\pi-A$ isotherms shifted to larger areas with increasing spacer length (n). Accordingly, the extrapolated areas of C*n*BP(FC14)$_2$ were 0.9, 1.3, 1.6, and 1.7 nm^2/molecule and were entirely more than ~0.28 × 2 = 0.56 nm^2 (cross-sectional area of one saturated fluorocarbon chain),[41] supporting their insolubility into water. These values suggest that longer spacers (n = 10 and 14) in C*n*BP(FC14)$_2$ may be flexible against lateral compression, judging from no areas proportional to spacer length. This flexibility was also supported by collapse behavior from the monolayer state. C*n*BP(FC14)$_2$ had a minimum value (35 mN m^{-1}, for n = 6) for collapse pressures, which can be judged from the inclination change of

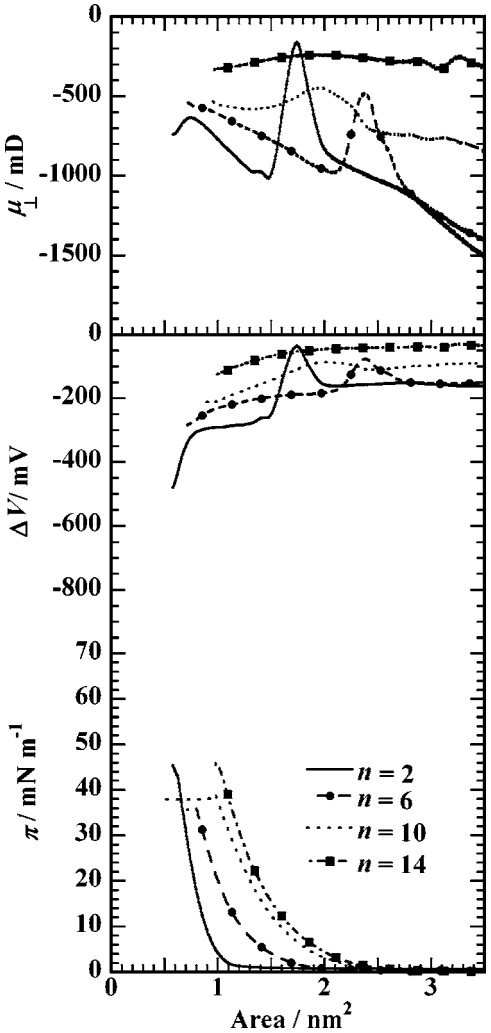

Figure 3. Surface pressure (π)−, surface potential (ΔV)−, and surface dipole moment ($\mu_\perp$)−area (A) isotherms of C*n*BP(FC14)$_2$ monolayers (n = 2, 6, 10, 14) on water at 298.2 K.

(41) Riess, J. G. In *Handbook of Fluorous Chemistry*; Gladysz, J. A., Horváth, I., Curran, D. P., Eds.; Wiley-VCH Verlag GmbH & Co. KGaA: Weiheim, 2004; pp 521−573. Krafft, M. P. In *Handbook of Fluorous Chemistry*; Gladysz, J. A., Horváth, I., Curran, D. P., Eds.; Wiley-VCH Verlag GmbH & Co. KGaA: Weiheim, 2004; pp 478−490.

the corresponding $\Delta V-A$ isotherms.[36,39,42−44] That is, the orientational mode of these monolayers on compression becomes different between $n \leq 6$ and $n > 6$. In the former case, the collapse pressures decreased with an increase in spacer length, which is quite reasonable in terms of the molecular ordering. C6BP(FC14)$_2$ forms a looser-packed monolayer in comparison to C2BP(FC14)$_2$ due to the longer hydrocarbon spacer. As for $n > 6$, however, the behavior contrary to the former one is observed. The collapse pressure of C14BP(FC14)$_2$ is higher than that of C10BP(FC14)$_2$. The higher collapse pressure means an enhancement of surface orientation of perfluorinated chains. In addition, there are few variations of ΔV values for C10BP(FC14)$_2$ and C14BP(FC14)$_2$ as molecular area decreases. In other words, the orientation of their fluorinated chains does not order in spite of lateral compression. These two results are divergent from each other. Therefore, there is the possibility that hydrocarbon spaces loop upon compression.

A surface potential (ΔV) generally traces the conformational change of alkyl chains to be oriented upward upon compression. A positive surface potential with a decrease in molecular area occurs for hydrogenated amphiphiles,[44] whereas negative changes appear for fluorinated ones.[45] In the case of $n = 2$ and 6, there appears a peak in the $\Delta V-A$ curve, which is experimentally reproducible. This suggests that the conformational change takes place in the monolayer state, although what kind of conformational change is occurring. The absolute surface potential ($|\Delta V|$) values, which were obtained by subtraction of the initial surface potential (ΔV_i) from the surface potential ($\Delta V_{close-packed}$) at the close-packed state, decreased with increasing spacer length. In the previous study,[43] $|\Delta V|$ value for perfluorotetradecanoic acid (FC14), which is the hydrophobic part of C*n*BP(FC14)$_2$, was ∼930 mV, except for the minor distinction caused by subphase composition. Compared to this value, all the absolute values of C*n*BP(FC14)$_2$ are quite small. This is because of less ordered orientational changes of fluorinated chains or other factors in relation to the conformational change in the hydrocarbon spacer upon compression. Considering the above-mentioned results for $\pi-A$ isotherms, however, the latter can be more possible.

The vertical component of surface dipole moments, $\mu_\perp$, was obtained by calculation using the Helmholtz equation:

$$\Delta V = \frac{\mu_\perp}{\epsilon\epsilon_0 A} + \psi_0 \tag{1}$$

where ϵ_0 is a permittivity of a vacuum (8.854×10^{-12} J^{-1} C^2 m^{-1}), ϵ the mean permittivity of monolayers (which is assumed to be 1), A the molecular area (nm^2), and ψ_0 the potential difference of the ionic double layer in ionized monolayers ($\psi_0 = 0$ for uncharged lipids). As for the charged monolayers such as FC14 and C*n*BP(FC14)$_2$ ($n = 2$, 6) on NaCl subphases, the ψ_0 value was calculated from the following equation:

$$\psi_0 = \frac{2kT}{\nu ze} \sinh^{-1}\left(\frac{\sigma}{\sqrt{2\epsilon\epsilon_0 n_0 kT}}\right) \tag{2}$$

where k is the Boltzmann constant, T the absolute temperature, ν the charge code of monolayers (±1), z the charge of monolayers, e the elementary charge, n_0 the number of ions per unit volume in the subphase, and σ the charge density(C m^{-2}). The $\mu_\perp$ value (∼−720 mD) of C2BP(FC14)$_2$ at the collapse was quite similar to that of FC14 (∼−690 mD), suggesting that conformations of hydrophobic chains for C2BP(FC14)$_2$ and FC14 are similar at the close-packed state. This behavior supports the above fact that the contribution of the spacer of $n = 2$ on the physicochemical property almost coincides with that of copper ions in their bulk properties.[37,38] On the other hand, other C*n*BP(FC14)$_2$ could respectively reach ∼550, ∼550, and ∼300 mD at the collapse state for $n = 6$, 10, and 14. Namely, their vertical components are smaller due to the effect of hydrocarbon spacers in comparison with those of C2BP(FC14)$_2$.

Effects of NaCl Subphase Concentrations. Figure 4 shows the representative $\pi-$, $\Delta V-$, and $\mu_\perp-A$ isotherms of C*n*BP(FC14)$_2$ monolayers spread on different concentrations of NaCl solutions at 298.2 K. The $\pi-A$ isotherms of C*n*BP(FC14)$_2$ shifted to smaller areas with increasing NaCl concentration (from 0.025 to 2.0 M NaCl). At the same time, they become closer to each other at higher surface pressures. Furthermore, there existed a kink point in their $\pi-A$ isotherms on NaCl solutions, which is different from that on water. This kink point corresponds to a first-order phase transition from disordered to ordered states as is mentioned in detail later. These transition pressures decrease with an increase in NaCl concentration, meaning that the NaCl addition to the subphase induces the condensation of C*n*BP(FC14)$_2$ monolayers. Their limiting molecular areas are ∼0.6 nm^2 (for $n = 2$, 6) and ∼0.7 nm^2 (for $n = 10$, 14). These values are almost the same as the above-mentioned cross-sectional area (∼0.6 nm^2) for two fluorinated chains. Figure 5 shows $\pi-$, $\Delta V-$, and $\mu_\perp-A$ isotherms of FC14 on NaCl subphases with different concentrations at 298.2 K. FC14 only cannot form a stable monolayer on water due to the solubility (data not shown) but can on NaCl subphases due to the salting out effect. The limiting molecular areas in Figure 5 are entirely ∼0.3 nm^2, which is in good agreement with the values of the previous data.[41,43] Accordingly, the $\pi-A$ isotherms in Figure 4 can be classified into two types by the limiting area and the shape of $\pi-A$ isotherms. As the first type, C2BP(FC14)$_2$ and C6BP(FC14)$_2$ have the same limiting area, the same transition pressure, and the same collapse pressure as those of FC14 (Figure 5). It means that C*n*BP spacers of C2BP(FC14)$_2$ and C6BP(FC14)$_2$ are exchanged for Na^+ ions just after spreading (Scheme 1). To clarify the dissociation of C*n*BP spacers, $\pi-$ and $\Delta V-A$ isotherms of FC14 were measured on 0.15 M NaCl subphase at 298.2 K (Figure 6). Superimposition of twice the FC14 molecular area and the C*n*BP(FC14)$_2$ area can allow better understanding their similarity. In addition, the $\Delta V-A$ isotherms nearly agree with each other in terms of both the absolute values and the shape. Although there are some differences between them, the differences might correspond to the contribution of dissociated C*n*BP spacers. Hence, such dissociation occurs for $n = 2$ and 6 just after spreading on NaCl subphases. In the second type, the $\pi-A$ isotherms of C10BP(FC14)$_2$ and C14BP(FC14)$_2$ moved stepwise to smaller areas with increasing NaCl concentration. Accordingly, their limiting areas also gradually changed with the subphase concentration. Their transition and collapse pressures were completely different from those of FC14. These differences demonstrate that no dissociation of C*n*BP counterions (n =10 and 14) from the monolayer occurs regardless of electrostatic interactions of the monolayer with Na^+ ions and of lateral compression. Moreover, ΔV values at the close-packed state became steadily more negative as NaCl concentration increased. Such values of C10BP(FC14)$_2$ on 1.0 M NaCl were more negative than those of C14BP(FC14)$_2$, although both limiting areas could reach twice the cross section of FC14 (∼0.6

(42) Hiranita, T.; Nakamura, S.; Kawachi, M.; Courrier, H. M.; Vandamme, T. F.; Krafft, M. P.; Shibata, O. *J. Colloid Interface Sci.* **2003**, *265*, 83−92.
(43) Nakahara, H.; Nakamura, S.; Kawasaki, H.; Shibata, O. *Colloids Surf. B* **2005**, *41*, 285−298.
(44) Nakahara, H.; Nakamura, S.; Nakamura, K.; Inagaki, M.; Aso, M.; Higuchi, R.; Shibata, O. *Colloids Surf., B* **2005**, *42*, 157−174.
(45) Broniatowski, M.; Dynarowicz-Latka, P. *J. Fluorine Chem.* **2004**, *125*, 1501−1507.

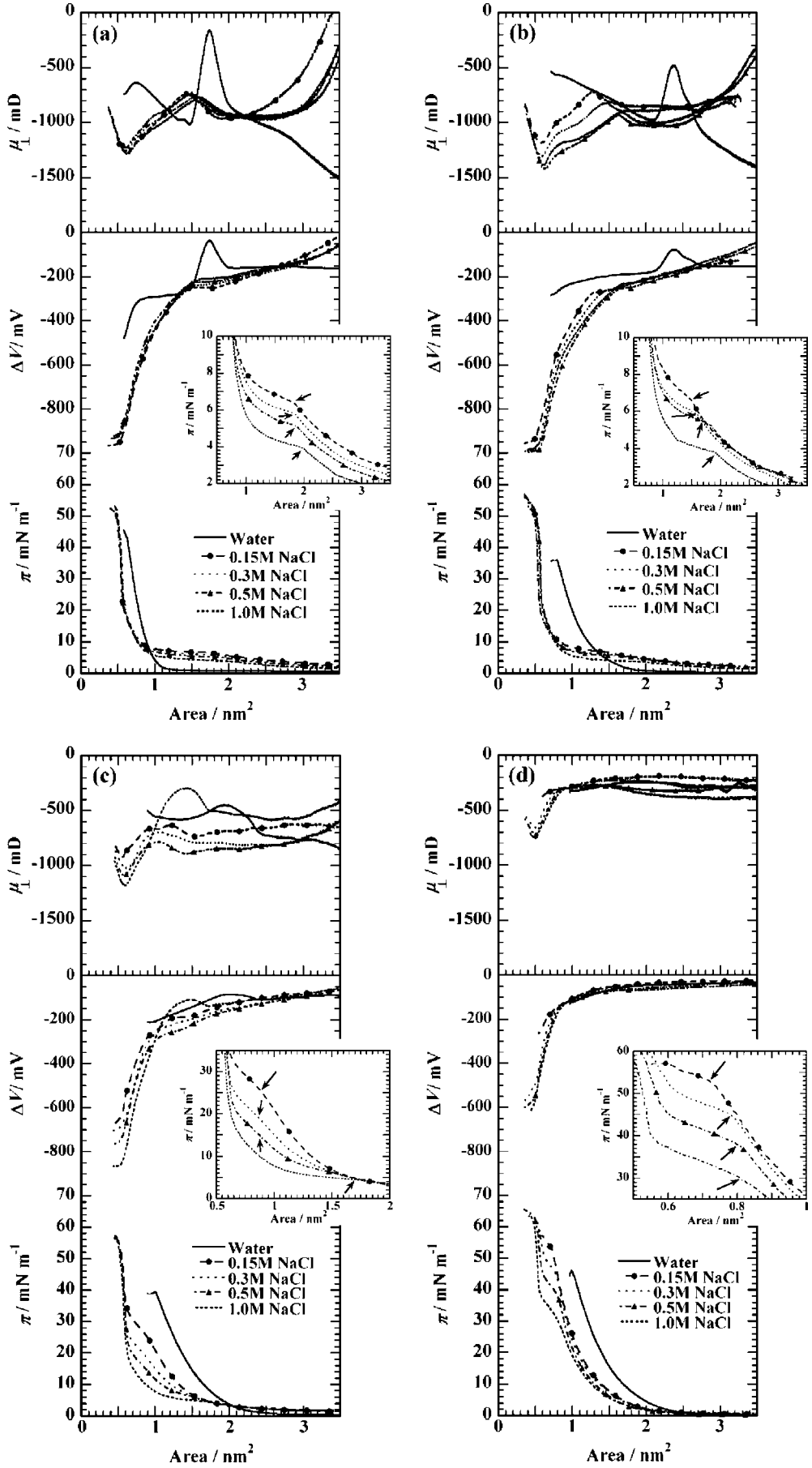

Figure 4. Surface pressure (π)−, surface potential (ΔV)−, and surface dipole moment ($\mu_\perp$)−area (A) isotherms of CnBP(FC14)$_2$ monolayers on NaCl subphases of different concentrations at 298.2 K; (a) $n = 2$, (b) $n = 6$, (c) $n = 10$, and (d) $n = 14$. (Inset) Enlarged $\pi-A$ isotherms in the transition regions, where the transition pressures are indicated by arrows.

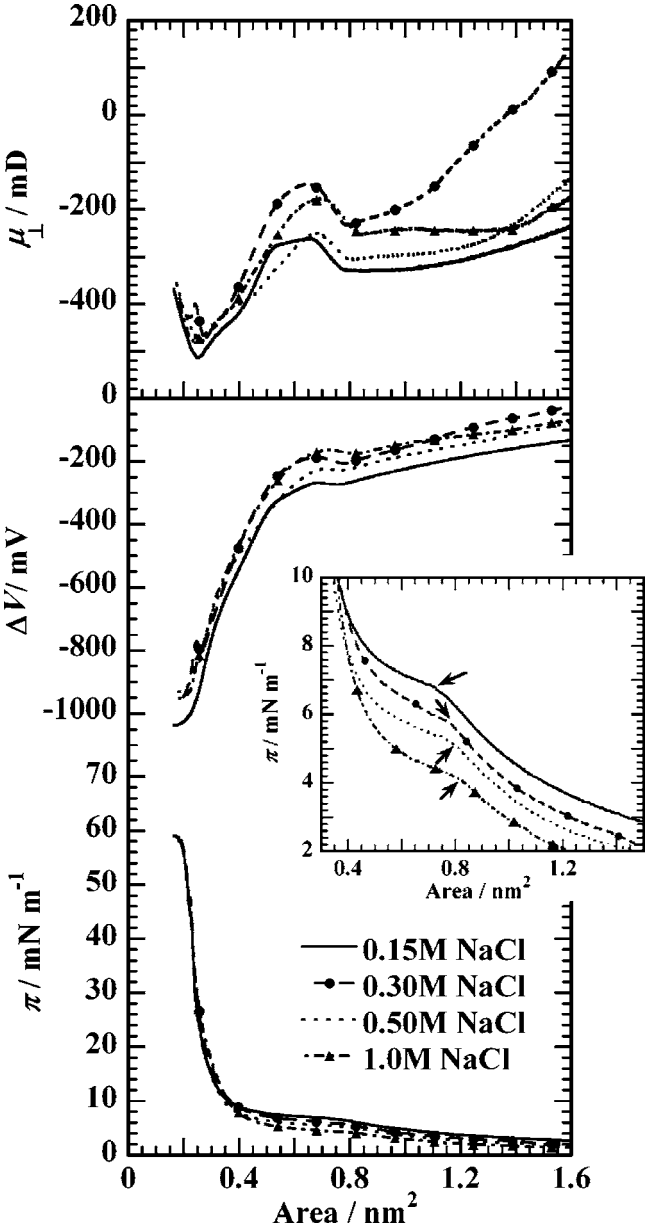

Figure 5. Surface pressure (π)−, surface potential (ΔV)−, and surface dipole moment ($\mu_\perp$)−area (A) isotherms of FC14 on NaCl subphases with different concentrations at 298.2 K. (Inset) Enlarged $\pi-A$ isotherms in the transition region, where the transition pressures are indicated by arrows.

Scheme 1. A Schematic Illustration of the Conformation for C*n*BP(FC14)$_2$ on NaCl at 298.2 K: (A) C*n*BP(FC14)$_2$, n = 2, 6; (B) C*n*BP(FC14)$_2$, n = 10, 14

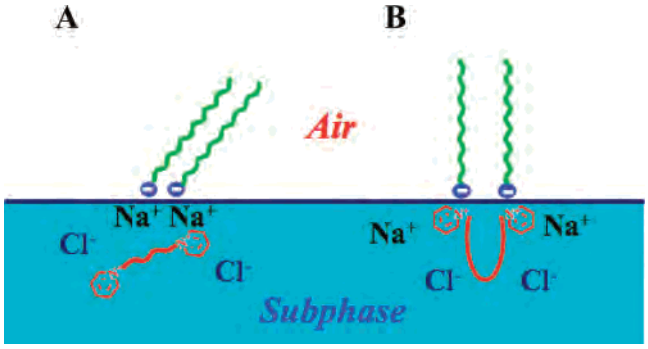

nm^2). This indicates that fluorocarbon chains of C10BP(FC14)$_2$ and C14BP(FC14)$_2$ are packed as closely as those of FC14 monolayers upon compression. That is, hydrocarbon spacers (n = 10, and 14) can be flexibly transformed to a certain folding or loop structure intruding into the subphase (Scheme 1), resulting in slight deviations of their limiting areas from 0.6 nm^2.

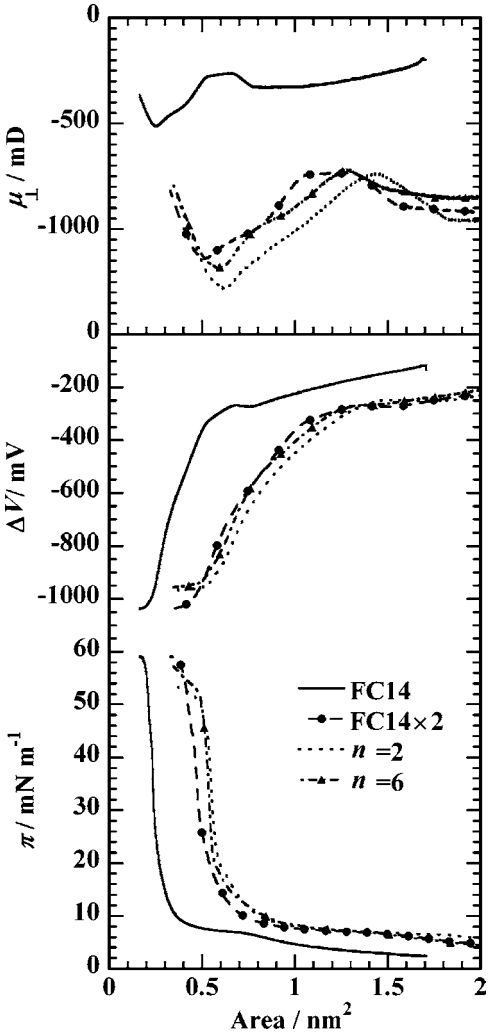

Figure 6. (a) Surface pressure (π)−, surface potential (ΔV)−, and surface dipole moment ($\mu_\perp$)−area (A) isotherms of FC14, twice amount of FC14, and C*n*BP(FC14)$_2$ (n = 2 and 6) on 0.15 M NaCl at 298.2 K.

Repeated Compression−Expansion Curves. Measurement of $\pi-A$ and $\Delta V-A$ isotherms under several compression and expansion cycles allows finding better information about the respreading ability, the reproducibility of surface behavior, and the formation of a different matrix. Figure 7 shows the repeated compression−expansion curves of C*n*BP(FC14)$_2$ on 0.15 M NaCl at 298.2 K. As for n = 2 and 6 in a and b of Figure 7, respectively, if C*n*BP counterions are dissociated not just after spreading but during compression, the second and third cycles in $\pi-A$ isotherm should be different from the first one. This is due to an easy exchange of the counterion, because the number of dissociated divalent counterions is much smaller than the number of Na^+ ions in the bulk. In fact, good reproducibility was obtained from the first to the third cycle, supporting the dissociation of the counterions immediately after spreading. Good reproducibility of $\pi-A$ curves (hysteresis) means location of C*n*BP^{2+} just near the interface.

In the case of n = 10 and 14, there were certain differences among the cycles. The transition area at ~26 mN m^{-1} in Figure 7c shifted to a smaller one with increasing the number of cycles, resulting from the lack of a respreading ability of monolayer

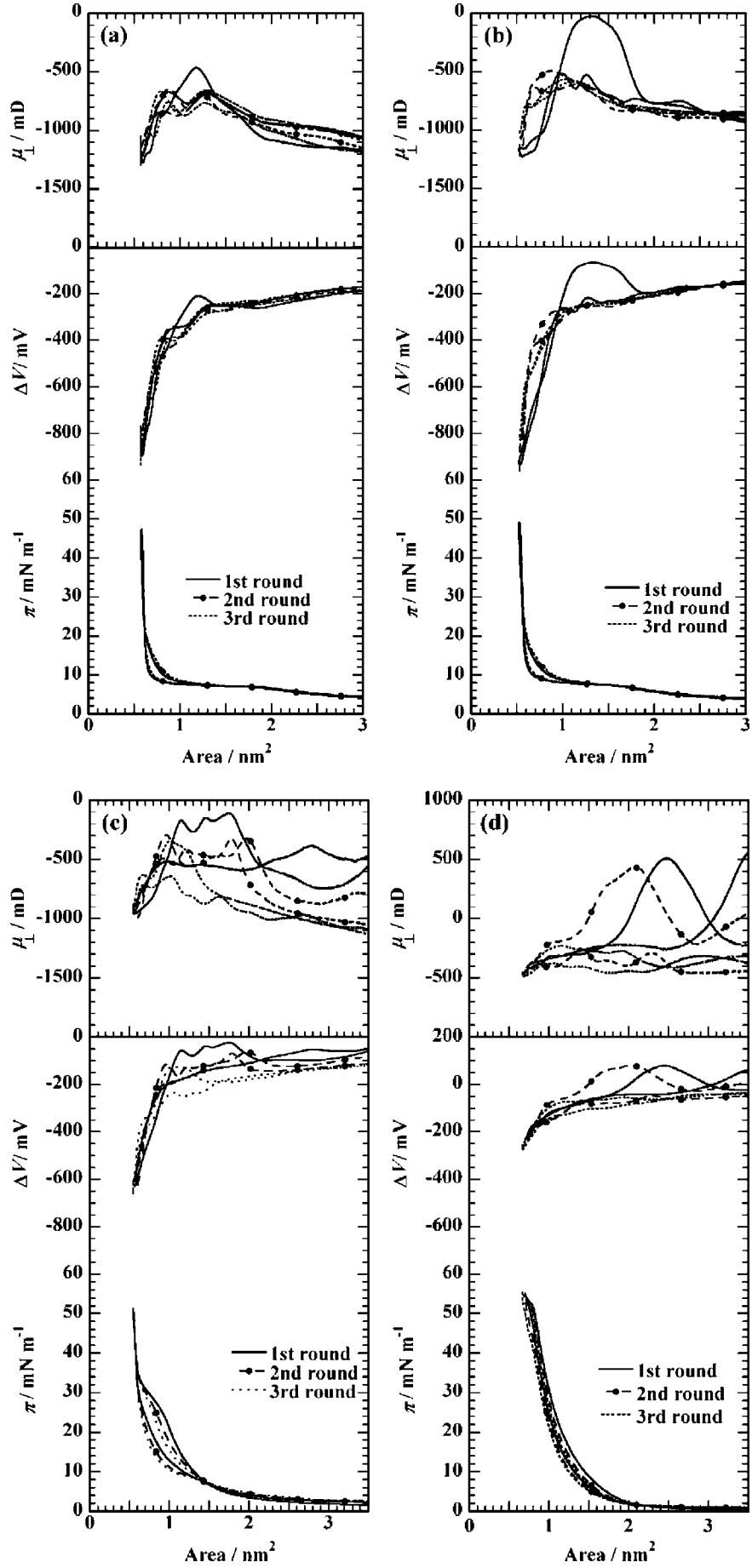

Figure 7. Cyclic compression and expansion isotherms of C*n*BP(FC14)$_2$ monolayers on 0.15 M NaCl at 298.2 K; (a) $n = 2$, (b) $n = 6$, (c) $n = 10$, and (d) $n = 14$. The measurements were carried out from first to third rounds.

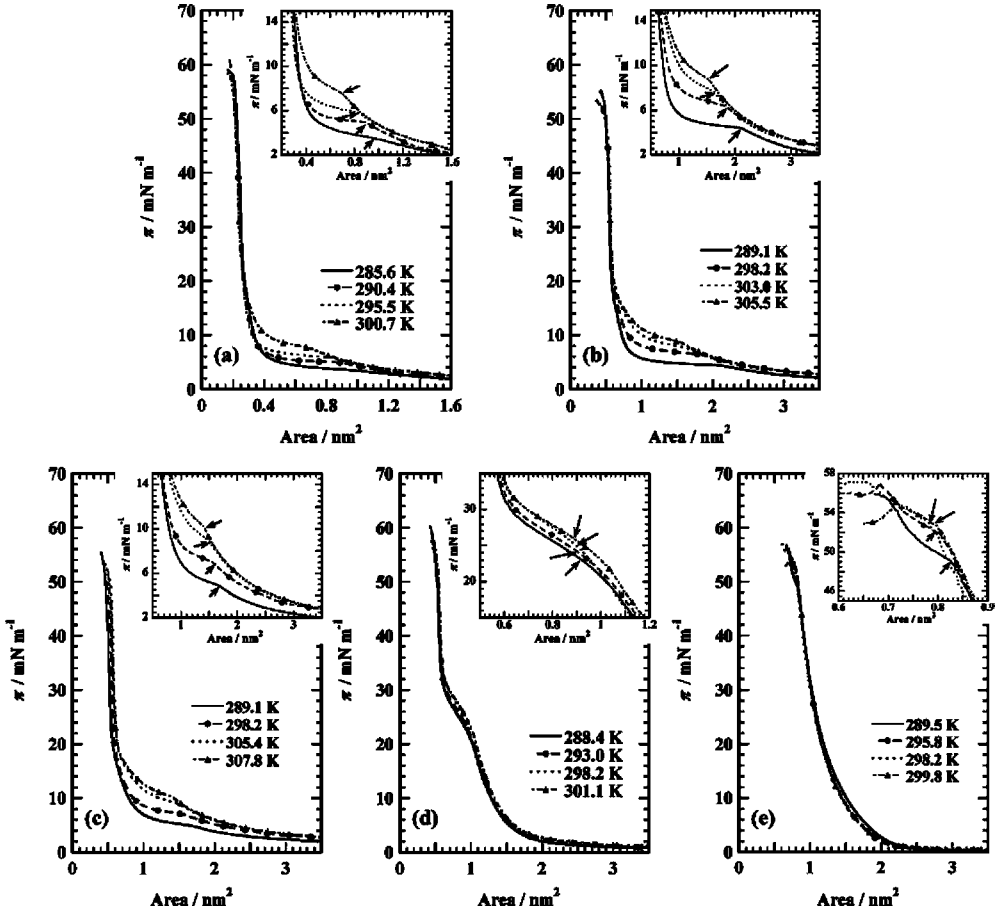

Figure 8. Temperature dependence of $\pi-A$ isotherms of (a) FC14, (b) C2BP(FC14)$_2$, (c) C6BP(FC14)$_2$, (d) C10BP(FC14)$_2$, and (e) C14BP(FC14)$_2$ monolayers. The $\pi-A$ isotherms were measured on 0.15 M NaCl at various temperatures. (Inset) Enlarged $\pi-A$ isotherms in the transition regions, where the transition pressures are indicated by arrows.

molecules. On the whole, however, the reproducibility of the limiting area and lift-off area from the first to the third cycles was also observed in Figure 7c,d. As mentioned in the former section, the counterions of C10BP(FC14)$_2$ and C14BP(FC14)$_2$ cannot be exchanged for Na^+ ions upon lateral compression. If such exchange happens during compression, there should be a difference between the first cycle and the second or third one in $\pi-A$ and $\Delta V-A$ isotherms. In other words, the second and the third rounds for $n = 10$ and 14 should coincide with the results of $n = 2$ and 6 in Figure 7 a and b, respectively. Judging from these results, however, it is demonstrated that the electrostatic attraction between the CnBP divalent cation ($n \geq 10$) and FC14 anion is quite strong even on NaCl subphases.

Apparent Molar Quantity Changes on the Phase Transition. A temperature dependence of the transition pressure (π^{eq}) of monolayers provides us with much interesting information. Figure 8 shows the $\pi-A$ isotherms of FC14 and CnBP(FC14)$_2$ on 0.15 M NaCl at different temperatures. All of these $\pi-A$ isotherms had a kink point at each temperature, showing the first-order phase transition from disordered states to ordered ones. This phase transition is also confirmed by morphological observations as described later (BAM and FM section). As can be easily expected, the transition pressures increased with increasing temperature. In addition, the collapse pressures decreased with an increase in temperature. The transition pressures as a function of temperature for CnBP(FC14)$_2$, FC14, and tetradecanoic acid (HC14) and for hydrogenated carboxylic acid as a representative of normal amphiphiles with a hydrocarbon chain[46] are plotted in Figure 9. Almost linear variations of the transition pressure against temperature were observed for all the compounds. It is widely accepted that the π^{eq} slope against temperature for fluorinated amphiphiles is smaller than that for hydrogenated ones due to the thermal stability of a fluorocarbon.[11,36] As is expected, the inclination of fluorinated compounds used in the present study is smaller. For CnBP(FC14)$_2$, the slope became slightly large as spacer length increased, resulting from the increase of intramolecular hydrocarbon parts. The obtained slopes can be used to evaluate the apparent molar quantity change in the phase transition. The evaluations for CnBP(FC14)$_2$ and FC14 are carried out by the previous manner,[32−36] which takes the contribution of the subphase to monolayers into account. The apparent molar entropy change (Δs^{γ}) on the phase transition is derived from the following equation:[46]

$$\Delta s^{\gamma}(\alpha,\beta) = (a^{\beta}-a^{\alpha})\,[(\partial\pi^{eq}/\partial T)_p - (\partial\gamma^0/\partial T)_p] \qquad (3)$$

where a^{α} and a^{β} are molecular areas (nm^2) of phase α and β, respectively. π^{eq} is the transition pressure from the α to the β state, and γ^0 is the surface tension of the subphase. The values of a^{α} and a^{β} are determined as follows. a^{α} is the area at the point where the monolayer starts to transform from the α to the β state. The a^{β} value is obtained in the following procedure; when the point (π^{eq},a^{α}) is moved to the zero area in parallel to the area axis, it comes into contact with the extrapolated line of the $\pi-A$ isotherm in the region of the ordered state. The intersection point is the a^{β} value. $\partial\pi^{eq}/\partial T$ is obtained from Figure 9, and $\partial\gamma^0/\partial T$

(46) Motomura, K.; Yano, T.; Ikematsu, M.; Matsuo, H.; Matsuura, R. *J. Colloid Interface Sci.* **1979**, *69*, 209−216.

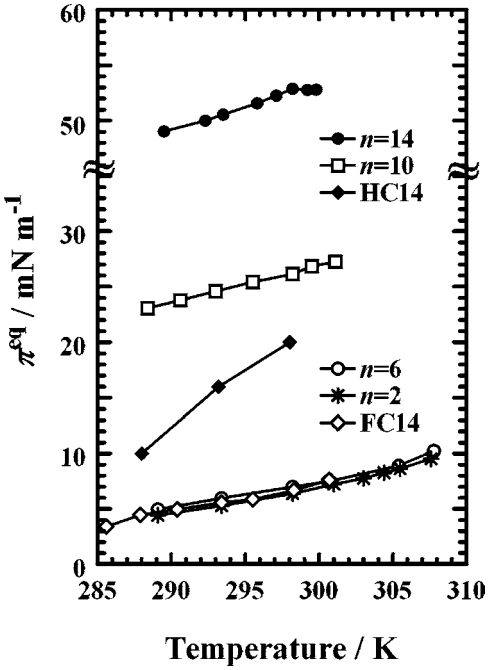

Figure 9. Changes in transition pressures (π^{eq}) against temperature on 0.15 M NaCl for $n = 2$; [C2BP(FC14)$_2$], $n = 6$; [C6BP(FC14)$_2$], $n = 10$; [C10BP(FC14)$_2$], $n = 14$; [C14BP(FC14)$_2$], FC14, and HC14.

Table 2. Apparent Molar Quantity Change on the Phase Transition at 298.2 K on 0.15 M NaCl

compound	Δs^{γ}/ (10^{-2} kJ K^{-1} mol^{-1})	Δh^{γ}/ (kJ mol^{-1})	Δu^{γ}/ (kJ mol^{-1})
HC14[a]	−4.7	−14	−17
FC14	−11	−33	−53
C2BP(FC14)$_2$	−31	−92	−140
C6BP(FC14)$_2$	−22	−65	−98
C10BP(FC14)$_2$	−7.8	−23	−39
C14BP(FC14)$_2$	−1.2	−3.6	−4.5
C14BP(HC14)$_2$[b]	−0.48 to −0.19	−1.43 to −0.57	

[a] On 0.15 M NaCl (pH 2) from refs 36 and 46. [b] On 4.4 M NaCl from ref 32.

is −0.16 on 0.15 M NaCl.[47−49] Furthermore, the apparent molar enthalpy change (Δh^{γ}) and energy change (Δu^{γ}) on the phase transition are evaluated by using eqs 4 and 5, respectively.[46]

$$\Delta h^{\gamma}(\alpha,\beta) = T\Delta s^{\gamma}(\alpha,\beta) \quad (4)$$

$$\Delta u^{\gamma}(\alpha,\beta) = -(\pi^{eq} - \gamma^{0})(a^{\alpha} - a^{\beta}) + T\Delta s^{\gamma}(\alpha,\beta) \quad (5)$$

The apparent molar quantity changes (Δs^{γ}, Δh^{γ}, and Δu^{γ}) for CnBP(FC14)$_2$, FC14, and HC14[36] on the phase transition at 298.2 K in 0.15 M NaCl are given in Table 2. All of the apparent molar enthalpies show negative values. Therefore, the transition from the disordered phase to the ordered one is exothermic. As for the apparent molar entropy, the values are completely negative as expected. With decreasing spacer length, the changes in Δs^{γ} become more negative, indicating that the ordered phases of C2BP(FC14)$_2$ and C6BP(FC14)$_2$ are in the closer-packed states. Note that the apparent molar entropy change of transfer from the disordered to the ordered phase for C6BP(FC14)$_2$ salt is the same as twice the change for FC14. Judging from the value of Δs^{γ}, the conformational state of C2BP(FC14)$_2$ is more ordered than those of C6BP(FC14)$_2$ and FC14. As for C14BP(FC14)$_2$ and C14BP(HC14)$_2$, which consist of the same CnBP spacer and tetradecane sulfonate moieties,[32] Δs^{γ} of C14BP(FC14)$_2$ indicates less negative value. Although there exist some differences in the experimental conditions, this distinction is attributed to bulkiness and weak intermolecular interaction of fluorocarbon chains.[50]

Brewster Angle Microscopy (BAM). The phase behavior of CnBP(FC14)$_2$ monolayers was morphologically investigated by Brewster angle microscopy (BAM)[51,52] and fluorescence microscopy (FM),[53] which provide direct information of the monolayers at the air−water interface. Figure 10 shows BAM images against surface pressures on 0.15 M NaCl at 298.2 K. As for FC14 in Figure 10a, the image at 5 mN m^{-1} indicates a homogeneous disordered phase. In the vicinity of its transition pressure (∼7 mN m^{-1}), ordered domains came to appear. On further compression, they grew in size as shown in Figure 10a from 10 to 20 mN m^{-1}, and then the images exhibited the complex pattern with bright edges. Such a pattern means the transformation from a 2-D to a 3-D structure, namely called a monolayer collapse at 40 mN m^{-1}. It is quite notable that ordered domains of FC14 are represented by darker contrast. Generally, for the monolayer of normal hydrocarbon amphiphiles, ordered domains reflect the emitted light differently than those from a subphase without monolayers.[52] Thus, ordered domains are visual in brighter contrast than disordered ones due to the difference in the reflectivity between them. However, the inverse contrast was observed for BAM images of the fluorinated compounds used here. In addition, the contrast between ordered domains and disordered regions was unfavorable compared to general BAM images.[54−56] These phenomena suggest that the disordered regions correspond to usual dark images and that the ordered domains represent darker ones due to the much lower reflective index of fluorinated amphiphiles.[57] Therefore, the ordered domains are recognized as relatively darker areas.

In the case of CnBP(CF14)$_2$ ($n = 2$ and 6), the images show the disordered phase at 5 mN m^{-1} and the coexistence state of the disordered and ordered phases at 10 and 20 mN m^{-1}. The shape of these domains looks like an ellipse (a bean). The changes of BAM micrographs with pressure for $n = 2$ and 6 are just the same as those of FC14. This also supports the dissociation of CnBP counterions in C2BP(FC14)$_2$ and C6BP(FC14)$_2$ on 0.15 M NaCl. For $n = 10$ and 14, the images varied in the same manner as above. Furthermore, the materials used in this study indicated the similar domain shape. However, the domains of C14BP(FC14)$_2$ become smaller in size and appear at higher surface pressures. In particular, the ordered domain of $n = 14$ indicated by arrows are much smaller. Moreover, the collapse pressures increase with increasing spacer length. Judging from the results of FC14, the behavior supports no dissociation of CnBP counterions (n =10 and 14) on compression. In addition, the similarity of these BAM results for CnBP(FC14)$_2$ to those for FC14 ensures that FC14 moieties in CnBP(FC14)$_2$ work as the hydrophobic part of monolayers.

(47) Jones, G.; Ray, W. A. *J. Am. Chem. Soc.* **1941**, *63*, 3262−3263.
(48) Shaw, D. J. *Introduction to Colloid and Surface Chemistry*; Butterworth-Heinemann: Oxford, UK, 1966; pp 1−196.
(49) Weast, R. C. *Handbook of Chemistry and Physics*, 48th ed.; Chemical Rubber Co.: Cleveland, OH, 1967−1968.
(50) Krafft, M. P. *J. Polym. Sci., Part A: Polym. Chem.* **2006**, *44*, 4251−4258.
(51) Henon, S.; Meunier, J. *Rev. Sci. Instrum.* **1991**, *62*, 936−939.
(52) Hoenig, D.; Möbius, D. *J. Phys. Chem.* **1991**, *95*, 4590−4592.
(53) McConnell, H. M. *Annu. Rev. Phys. Chem.* **1991**, *42*, 171−195.
(54) Möbius, D. *Curr. Opin. Colloid Interface Sci.* **1998**, *3*, 137−142.
(55) Gehlert, U.; Weidemann, G.; Vollhardt, D. *J. Colloid Interface Sci.* **1995**, *174*, 392−399.
(56) Lee, Y.-L.; Lin, J.-Y.; Chang, C.-H. *J. Colloid Interface Sci.* **2006**, *296*, 647−654.
(57) Dean, J. A., Ed. *Lange's Handbook of Chemistry*, 13th ed.; McGraw-Hill: New York, 1985; pp 1−1792.

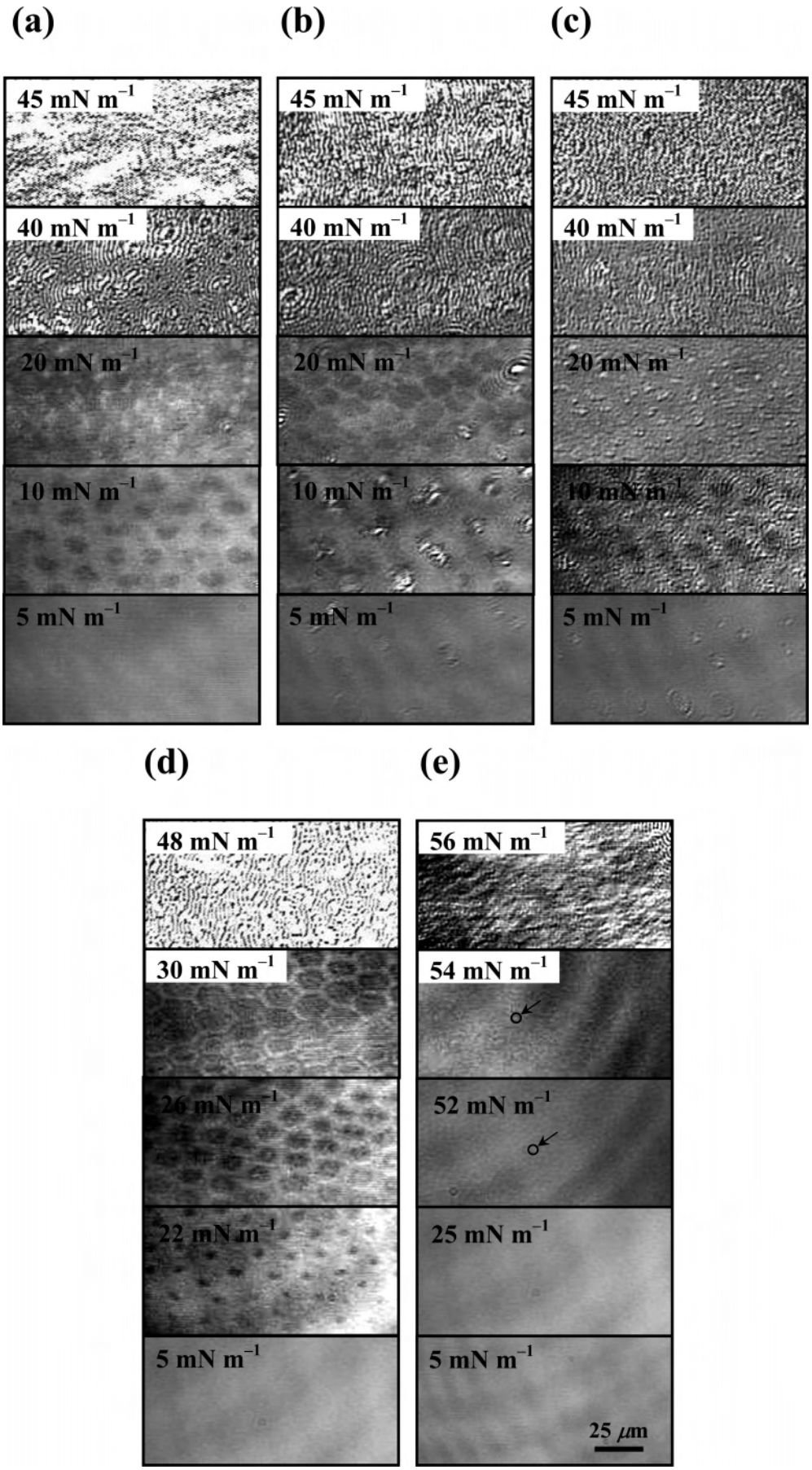

Figure 10. BAM images of (a) FC14, (b) C2BP(FC14)$_2$, (c) C6BP(FC14)$_2$, (d) C10BP(FC14)$_2$, and (e) C14BP(FC14)$_2$ monolayers at selected surface pressures. The representative ordered domains of C14BP(FC14)$_2$ monolayers were indicated by arrows at 52 and 54 mN m^{-1}. The scale bar represents 25 μm.

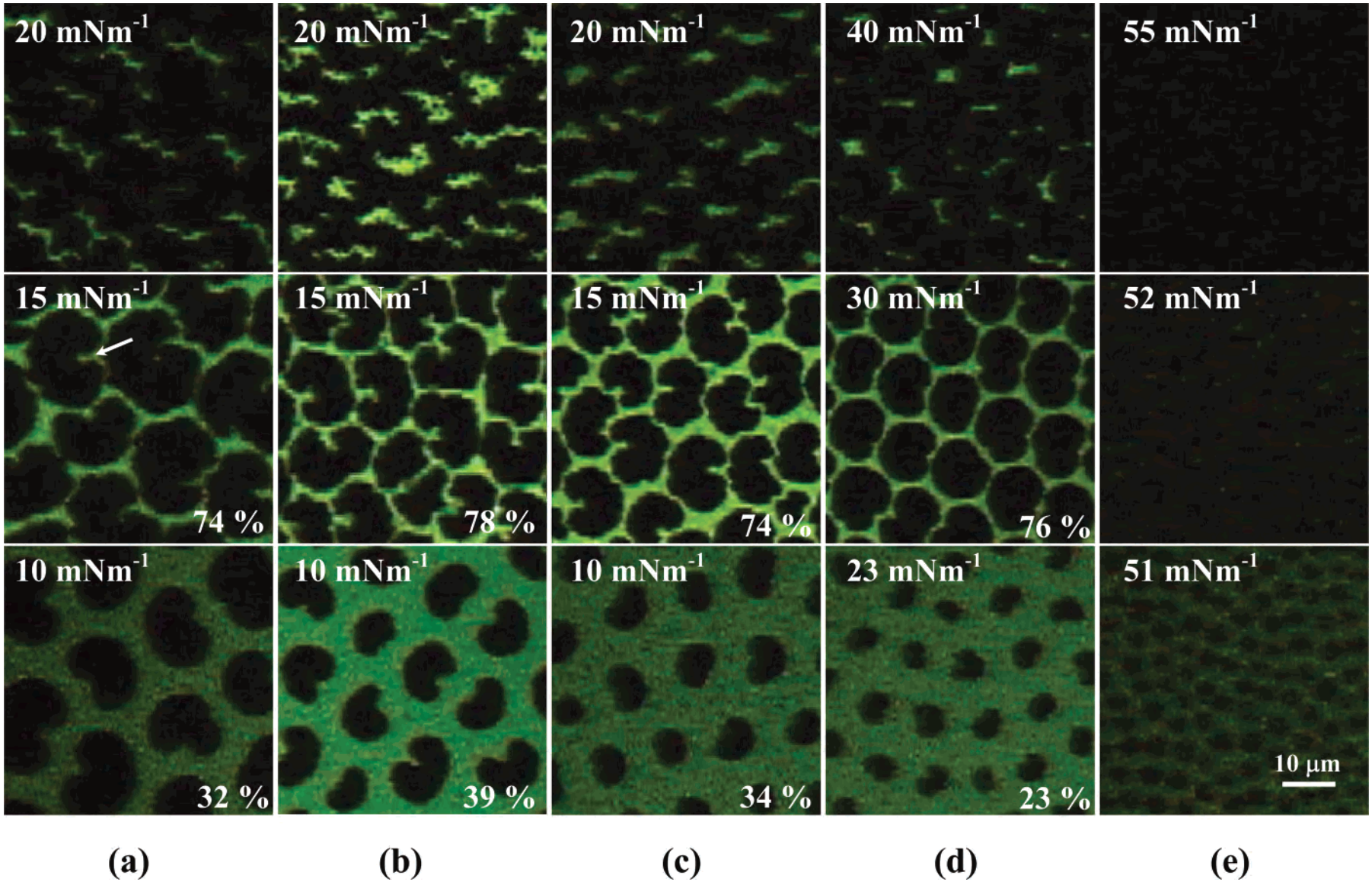

Figure 11. FM micrographs of (a) FC14, (b) C2BP(FC14)$_2$, (c) C6BP(FC14)$_2$, (d) C10BP(FC14)$_2$, and (e) C14BP(FC14)$_2$ monolayers at selected surface pressures. The percentage in the lower right refers to the ratio of ordered phases in the micrograph to the flame area. The monolayers contained 1 mol % of fluorescent probe (NBD-PC). The typical defect of FC14 ordered domains was indicated by an arrow. The scale bar represents 10 μm.

Fluorescence Microscopy (FM). Fluorescence microscopy measurement needs adequate probes in the monolayer and thus provides us direct images. Although there is a possibility that FM probe molecules affect the essential phase behavior of monolayers, it can become negligible by adding just a small amount of the probes to monolayers, which has no influence on the original $\pi-A$ and $\Delta V-A$ isotherms, and domain shapes in BAM micrographs. Nevertheless, FM generates quite higher-contrast, higher-resolution, higher-magnification, and strain-free pictures in comparison to those generated by BAM. Shown in Figure 11 are FM images of FC14 and C*n*BP(FC14)$_2$ on 0.15 M NaCl at 298.2 K. As for FC14, homogeneous bright images were observed at $<\sim 7$ mN m^{-1} (data not shown), corresponding to disordered regions in Figure 11a. Black domains (ordered domains) started to appear at the transition pressure ($\sim$7 mN m^{-1}), and then they grew in size as surface pressures increased. Finally, the micrographs became homogeneously dark because of a concentration quenching of FM probes or a close-packed state of ordered monolayers.[58] The image at 10 mN m^{-1} included beanlike ordered domains of ~ 10 μm in diameter. Upon further compression, the domains became large in size (~ 15 μm in diameter) at 15 mN m^{-1}, and a ratio of ordered domains to this picture increased from 32 to 74%. Note that the defect of ordered domains indicated by an arrow directs to the compressing direction. This might result from the convection upon compression. The similar variations of FM images were observed for $n = 2$ and 6. The domain size of C2BP(FC14)$_2$ and C6BP(FC14)$_2$ became slightly small in comparison to that of FC14, attributing to the effect of the dissociated C*n*BP counterions as mentioned in the previous section. The variations of FM images for $n = 2$ and 6 almost agree with those of FC14 at the corresponding BAM micrographs. Therefore, the exchange of the counterions ($n = 2$ and 6) by Na^+ ions is also supported. Accordingly, the phase behavior of FC14 monolayer on 0.15 M NaCl is also observed for $n = 2$ and 6.

In the case of $n = 10$, the domain of ~ 10 μm in diameter at 30 mN m^{-1} indicated more circular shapes than that of $n = 2$, 6 and FC14. This change in domain shape suggests that the interfacial property of C10BP(FC14)$_2$ is different from that of C2BP(FC14)$_2$ and C6BP(FC14)$_2$. Similarly, as for $n = 14$, the circular ordered domains of ~ 3 μm in diameter appeared at 51 mN m^{-1}. Thus, it is demonstrated that the phase behavior of C10BP(FC14)$_2$ and C14BP(FC14)$_2$ differs much from that of FC14. Therefore, their C*n*BP counterions can be said not to dissociate from the hydrophobic monolayer regardless of lateral compression.

In addition, a magnitude of lens is 50 times for FM, while that of BAM is 10 times; therefore, images for FM are much clearer and more reliable. The real shape of the domain is bean-like, based upon FM images.

Conclusions

Newly synthesized 1,1-(1,ω-alkanediyl)-bispyridinium perfluorotetradecane carboxylate [C*n*BP(FC14)$_2$, $n = 2$, 6, 10, 14] can form a stable monolayer on water at 298.2 K. The new finding in the present study is that the interfacial behavior of C*n*BP(FC14)$_2$ monolayers on water and NaCl subphases is completely different between shorter ($n = 2$, 6) and longer spacers ($n = 10$, 14). On 0.15 M NaCl, in particular, C*n*BP(FC14)$_2$ with the shorter spacers ($n = 2$, 6) shows the dissociation of their C*n*BP counterions. As for the longer spacers ($n = 10$, 14), on the other hand, no dissociation of C*n*BP occurs with folding of the spacer upon compression. This phenomenon was supported by the similarity of Langmuir isotherms and morphological observations (BAM and FM) to those for perfluorotetradecanoic acid (FC14) which is the hydrophobic moiety of C*n*BP(FC14)$_2$. In addition, it is also confirmed by repeated compression−expansion cycle curves of each C*n*BP(FC14)$_2$. From thermodynamic analyses, the fluorinated chains are packed more closely as the spacer length becomes shorter. It is further demonstrated that C*n*BP(FC14)$_2$ chains are in more constraint at the close-packed state of monolayers than the corresponding hydrogenated analogues.

Acknowledgment. This work was supported by a Grant-in-Aid for Scientific Research 17310075 from the Japan Society for the Promotion of Science and by Grant 17650139 from the Ministry of Education, Science and Culture, Japan, and by Japan-Taiwan Joint Research Program, which are gratefully acknowledged. This work (H.N.) was also supported by Research Fellowships of the Japan Society for the Promotion of Science for Young Scientists (18.9587).

LA700511R

(58) Maruta, T.; Hoda, K.; Inagaki, M.; Higuchi, R.; Shibata, O. *Colloids Surf., B* **2005**, *44*, 123−142.